

Multiscale Crystal Plasticity Modeling based on Field Theory

T. Hasebe¹

Abstract: This paper presents recent achievements in field theoretical approach toward substantial linkage among key hieratical scales dominating polycrystalline plasticity of metals and alloys. Major ingredients of the theory are briefly shown first, which is followed by several overwhelming results and some implications including key factors for dislocation cell structure evolution, key features of polycrystalline plasticity and their rational modeling in crystal plasticity-based constitutive equation.

keyword: Multi-scale modeling, Field theory, Crystal plasticity, Dislocation theory, Strain gradient plasticity

1 Introduction

Recent attempts in simulating plasticity-related phenomena over two or more scales have tended to blindly toward “enhancement of spatial-temporal simulation scales” based on simple reducibility concept. Methods often mentioned in this context are nothing more than an enumeration of *ab initio* calculations, and classical molecular dynamics (MD) method, discrete dislocation dynamics (DDD), and crystal plasticity [e.g., Tomson, et al.(2002), Ghosh (2002), Ghoniem and Cho (2002), Zbib and Diaz de la Rubia (2002)]. What is generally lacking there would be a correct set of epistemology of the related phenomena, especially mechanical responses under complex loading conditions including high strain rate, non-proportional straining paths, etc., and resultant evolutions of dislocation substructures. Experimental observations and related investigations strongly imply that these complicated-looking materials responses can be treated in a unified manner with relatively simple models from a viewpoint of dislocation substructure evolutions. This seems to be out of scopes and even far beyond the reach both from those methods and approaches based on atomistic and continuum mechanics viewpoints.

This paper describes overview of field theoretical approach toward multiscale crystal plasticity recently

achieved by the author’s group. The theory provides essentially new viewpoints to look into the overall multi-scale approach in the completely new light, which will be given below with some typical results.

2 Overview of Field Theory of Plasticity

The author has advocated “field theory of plasticity [Hasebe and Imaida (1998), Hasebe and Imaida (1999a)]” motivated by the stagnation of the theoretical progress in recent plasticity. Although the theory has not been conclusive yet, it has suggested many important implications. Basic structure of the theory is tentatively composed of (A)continuum description of inhomogeneous fields including dislocations and defects based on the differential geometrical field theory, often referred to as “non-Riemannian plasticity,” and (B)field theoretical descriptions of collective behavior of interacting dislocations, defects and crystal grains. This two-fold structure interrelated by gauge field theory is shown in Fig.1. The (A) concerns with describing scale effects and evolution of the scales and it principally covers all the aspects of the strain gradient plasticity accommodating “inhomogeneities” and the related “scale effects” of the fields. The (B), on the other hand, describes “evolution” of the fields which is normally missing in any of the conventionally proposed theories. In what follows, the basic concepts and major results regarding (A) and (B) together with gauge field theory will be briefly presented.

2.1 Differential Geometrical Field Theory

Since essentials of plasticity of metallic materials are motions and interactions of crystallographic imperfections, i.e., dislocations and defects existing within crystalline space, it is quite natural and rational for us to use differential geometrical language in describing them. “Torsion” of the crystalline space corresponds to dislocations, while the “curvature” describes all the other kinds of defects including not only simple ones like dislocation dipole, vacancy, foreign atoms, and precipitates,

¹ Kobe University, Hyogo, Japan. hasebe@mech.kobe-u.ac.jp

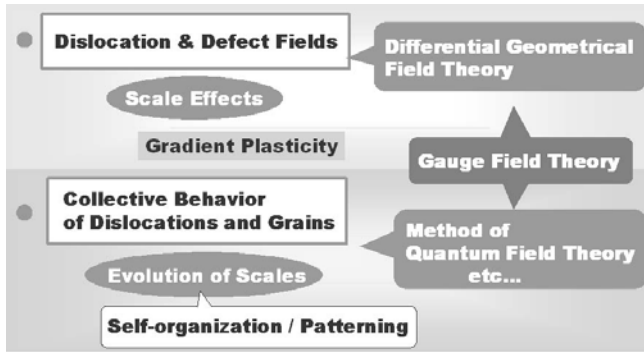


Figure 1 : Two-fold construction of field theory of plasticity interrelated by gauge field theory.

but also complicated fields including dislocation substructures such as ladders, veins, labyrinths and cells. The important thing is that these quantities are expressed as gradients of distortion or strain tensor in the context of continuum mechanics, meaning the theory intrinsically requires “strain gradients” at least up to the second order. Torsion and curvature tensors are defined respectively as,

$$S_{kl}^{..j} = \Gamma_{[kl]}^j$$

$$R_{klm}^{..n} = 2 \left[\partial_{[k} \Gamma_{l]m}^n + \Gamma_{[k|p]}^n \Gamma_{l]m}^p \right] \quad (1)$$

where Γ_{kl}^j indicates coefficient of connection. Contractions of these higher order tensors considering the symmetry result in well-known second rank tensors. They are respectively called “dislocation density tensor” and “incompatibility tensor” given respectively by a curl of distortion tensor and double curl of strain tensor, i.e.,

$$\alpha_{ij} = \epsilon_{ikl} \partial_k \beta_{lj} = \frac{1}{2} \epsilon_{ikl} S_{kl}^{..j} \quad (2)$$

$$\eta_{ij} = -\epsilon_{ikl} \epsilon_{jmn} \partial_k \partial_m \epsilon_{ln} = \frac{1}{4g} \epsilon_{ikl} \epsilon_{jmn} R_{klm}^{..n} \quad (g = \det(g_{ij}))$$

As demonstrated below, the dislocation density tensor “includes” but is not limited to the recently popular concept of “geometrically-necessary” types of dislocations. Note, the energy duals of these quantities mathematically introduce the physical counterparts, i.e., couple stress tensor and stress function tensor [Hasebe and Imaida (1999)].

2.2 Method of Quantum Field Theory

One of the most prominent outputs of the field theoretical approach would be the successful reproduction of dislocation cell structures [Hasebe and Imaida (1998), Hasebe

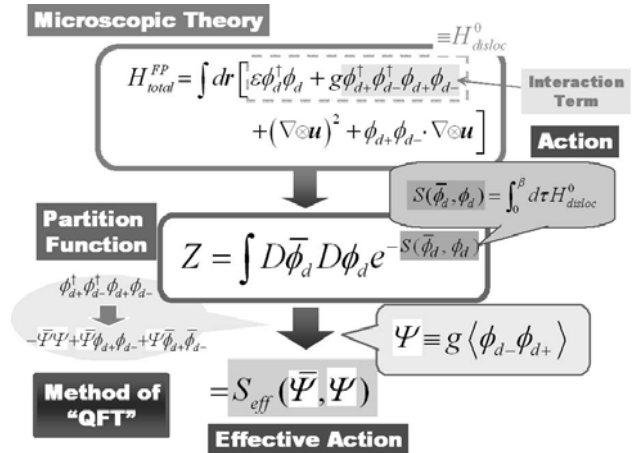


Figure 2 : Schematic for derivation procedure of effective theory for cell formation based on the method of quantum field theory (QFT).

(2004)] based on an effective theory rigorously derived from a dislocation theoretical microscopic theory. Here a use was made of the method of quantum field theory (QFT), which is mathematically equivalent to statistical mechanics, providing a rigorous derivation through systematic “coarse-graining” and renormalization of scales. The point of departure of the derivation is to write down the Hamiltonian of the dislocation system embedded in a crystalline space determined based on the gauge field theory briefly given below.

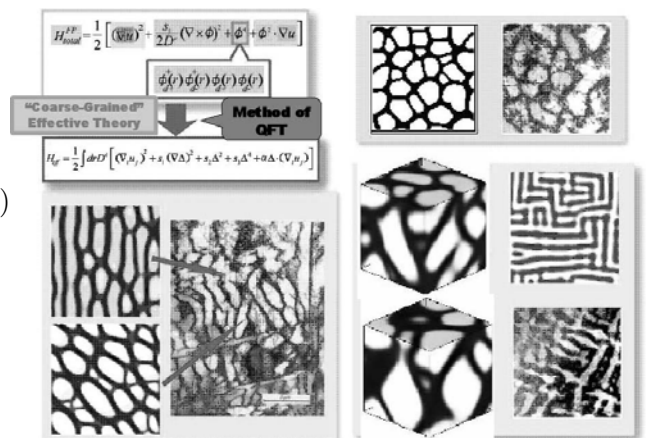


Figure 3 : Simulated 2D and 3D dislocation cell structures based on the method of quantum field theory (QFT).

Figure 2 displays the derivation procedure starting from the dislocation theoretical first principle Hamiltonian of the system H_{total}^{FP} , which is given as a sum of pure elas-

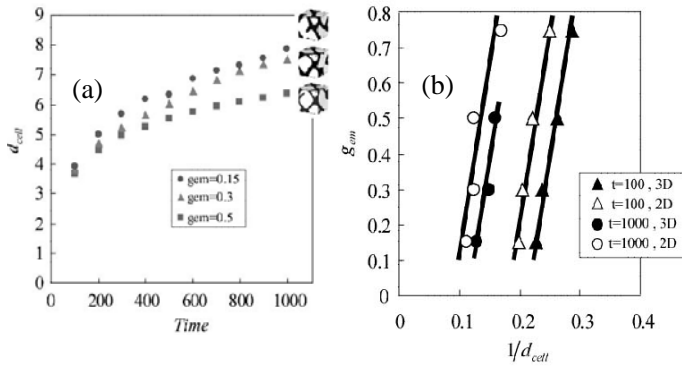


Figure 4 : Simulation results for (a)cell size evolution with time step and (b)relationship between gem and inverse cell size.

tic, pure dislocation and their coupling terms. Second quantized form of the Hamiltonian for the pure dislocation system incorporating dislocation pair interaction by a quartic term $\hat{\phi}_{d+}^\dagger \hat{\phi}_{d+} \hat{\phi}_{d+}^\dagger \hat{\phi}_{d+}$ is considered. Regarding the pair interaction as pair annihilation processes responsible for dynamic recovery, the energy expectation value for the interaction $g \langle \phi_{d+} \phi_{d-} \rangle$ is introduced and is used as an order parameter of the coarse-grained system.

A digest of the simulation results are shown in Figs.3 and 4. They provide many implications, e.g., (1)dislocation interaction relating to pair annihilations and its collective effect lead to modulation in dislocation distribution instead of the uniform distribution, (2)long range internal stress field plays the key role in evolution of the cellular morphology, and directly determines the size, without which “far-from-cell” structures will possibly result.

2.3 Gauge Field Theory

Although the above-stated differential geometrical descriptions of dislocations and defects are natural in expressing them, their practical usages are not always self-evident in their own theoretical framework. Gauge field theory, on the other hand, gives a clear guideline in a mathematical sense. The theory substantially puts its basis on elasticity of crystals, and dislocations and defects are introduced as “gauge fields” in an elastically deforming crystalline body to satisfy the requirement of invariance of the Lagrangian of the system under the local gauge transformation specified by $G = T(3) \triangleright SO(3)$. This is called “minimum replacement” with which the following covariant differentiation is introduced. Consider solely the dislocation field $T(3)$ for simplicity, the

covariant derivative is given by,

$$D_a x^i = \partial_a x^i + \phi_a^i \equiv B_a^i \quad (3)$$

where ϕ_a^i represents gauge field corresponding to dislocation. Since the covariant derivative is acting on the coordinate cover, the derivative expresses distortion tensor. Thus strain tensor is defined as,

$$\begin{aligned} E_{AB} &= \frac{1}{2} \left(B_A^i \delta_{ij} B_B^j - \delta_{AB} \right) \\ &= \frac{1}{2} \left\{ (\partial_A x^i + \phi_A^i) \delta_{ij} (\partial_B x^j + \phi_B^j) - \delta_{AB} \right\} \\ &= \frac{1}{2} \left\{ \partial_A x^i \partial_B x^i + \phi_A^i \phi_B^i + 2\phi_{(A}^i \partial_{B)} x^i - \delta_{AB} \right\} \end{aligned} \quad (4)$$

where A runs 1 through 3 and the subscript 4 means time. The Lagrangian for the elastic body containing dislocations is thus given by,

$$\begin{aligned} L_{elastic} &= T(B_4^i) - V(E_{AB}) \\ &= \frac{1}{2} \rho_0 B_4^i \delta_{ij} B_4^j - \frac{1}{2} D_{ABCD}^e E_{AB} E_{CD} \end{aligned} \quad (5)$$

The strength of the dislocation field is called “curvature” of the gauge field defined as,

$$D_{ab}^i = \frac{1}{2} (\partial_a \phi_b^i - \partial_b \phi_a^i) = \partial_{[a} \phi_{b]}^i \quad (6)$$

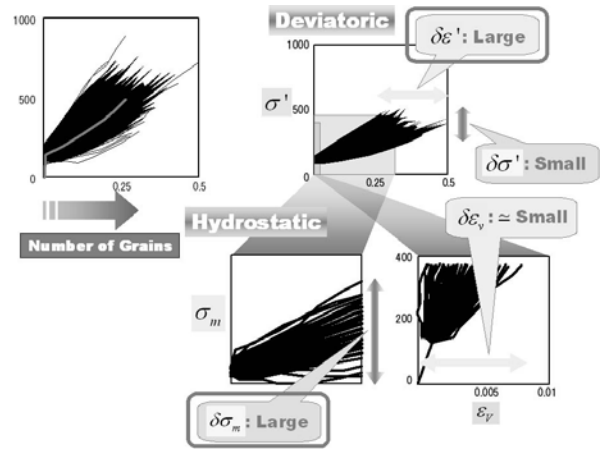


Figure 5 : Schematics showing “collective effect” of crystal grains for polycrystalline plasticity characterized by field fluctuations.

A gauge invariant Lagrangian for the dislocation field is

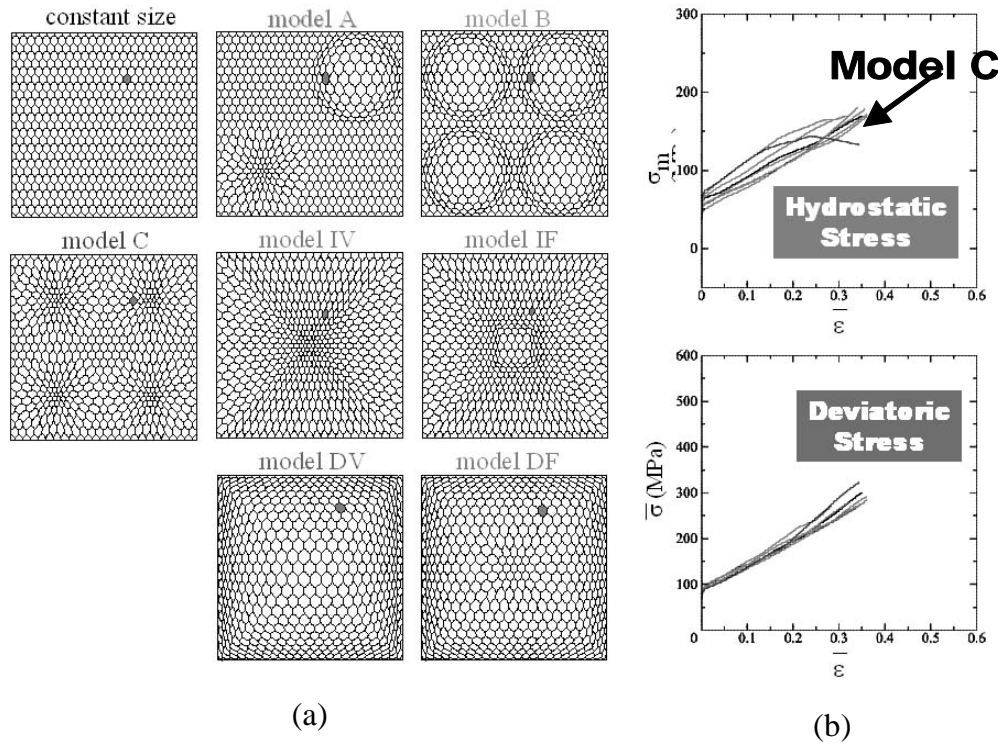


Figure 6 : Grain size distribution models together with stress response of a grain located relatively in the same position for all the models.

defined by the quadratic form of the curvature as,

$$L_{disloc} = -\frac{1}{2}\delta_{ij}D_{ab}^i k^{ac} k^{bd} D_{cd}^j$$

$$= -\frac{1}{4}k^{ac} k^{bd} \partial_{[a} \phi_{b]}^i \partial_{[c} \phi_{d]}^j \quad (7)$$

where $k^{AB} = -\delta^{AB}$ and k^{44} represents inverse of shear wave velocity. The total Lagrangian is given by the sum of the above two, and the Legendre transformation gives the corresponding Hamiltonian which provides the point of departure for the use of QFT described in 2.2. Note, as far as we regard the dislocations and defects as internal degrees of freedom, we do not have to care about the annoying higher order boundary conditions.

3 Applications to Polycrystalline Plasticity

3.1 Collective Effect of Crystal Grains

Important as well as intriguing finding recently obtained is about polycrystalline plasticity. A series of analyses based on systematically designed FE polycrystal models with increasing number of composing grains has revealed many implications crucial in substantial modeling

of polycrystalline aggregates. Large fluctuations in hydrostatic stress and deviatoric strain are observed as the number of grains increases, which is one of the primary manifestations of the collective effect of grains. Note that the viewpoint of “field fluctuations” is applicable to more realistic and complicated situations where grain size distribution and/or second phases exist, which will be presented in 3.2 and 3.3, respectively. Figure 5 summarizes the results relating to the field fluctuations. For further details, see [Hasebe (2004a), Hasebe(2004b)].

3.2 Roles of Grain Size Distribution

The field theoretical approach has also clarified the roles of grain size distribution in polycrystalline plasticity of metals recently. Finite element polycrystal models comprising 613 grains with systematically designed grain size distributions are mainly used in this series of studies, where the same relative combinations of the crystallographic orientations are set in common to all the models together with a 23-grain sensing area embedded in the central part. Roughly two types of size distributions are assumed to simplify the discussion as shown in Fig.6(a),

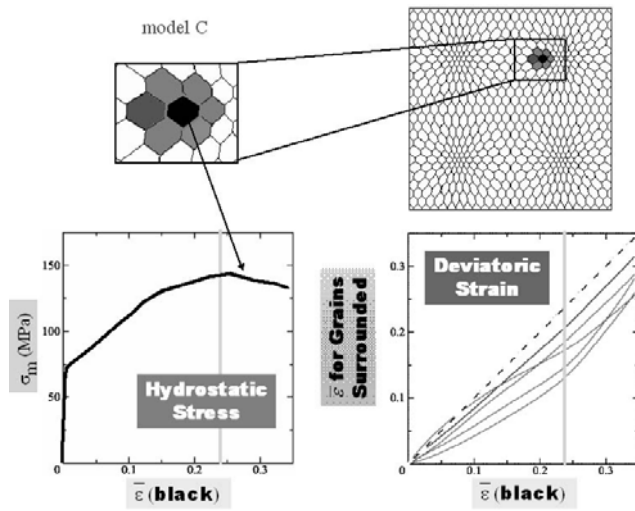


Figure 7 : Irregular change in hydrostatic stress caused by its inhomogeneous distribution within grain, which results in stress redistribution to the surrounding grains promoting additional local plastic flow.

i.e., models with global size distribution over the sample with increasing or decreasing grain diameter (Models IV, IF and Models DV, DF), and those with localized size changes (Models A to C).

A two slip-system plane strain crystal plasticity model is used to introduce the highest constraint to the grain deformations for the purpose of maximizing the collective effect. The effect of the grain size distribution on stress and strain distributions in the sensing area is examined. The global size distributed models exhibit relatively large deviation of the stress and strain distributions from those for the constant size model, whereas the localized distribution models yield small deviation.

Details of the interrelationship between the fluctuations in hydrostatic stress and deviatoric strain are extensively discussed. One of the typical results is shown in Fig.6(b) where stress responses of a grain located in the same relative positions are compared among the models. Hydrostatic stress tends to yield irregular change during the course of plastic deformation in general, whereas deviatoric stress basically shows monotonic increase regardless of the models. Figure 7 picks up the Model C’s hydrostatic stress response, together with deviatoric strain response of the surrounding six grains. The figure implies the saturation of the hydrostatic increase corresponds to rate changes in deviatoric strain of the surrounding grains. The irregular response in hydrostatic

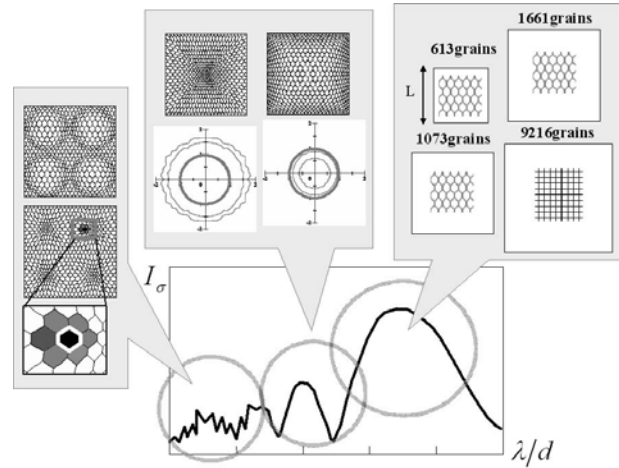


Figure 8 : Summary of grain size distribution effect on polycrystalline plasticity in terms of frequency analysis of stress fluctuation.

stress stems from heterogeneous deformation of the underlying grain mainly attributed to the deviated grain shape from hexagon, and redistributions of the hydrostatic stress occur upon relaxation of the heterogeneously distributed intra-granular stress which consequently promotes additional plastic deformations in the surrounding grains.

A discussion is also made on the characteristics of the global stress fluctuations together with the dependency on grain size distribution. As summarized in Fig.8, a modified Fourier analysis reveals that there exists predominant long range wavelength in the stress spectrum comparable to the size of the sample regardless of the grain size distribution. The global grain size distribution mainly influences the second maximum spectrum of the order of 10 grains, while the further details of the size distribution essentially affects smaller spectrum region less than 19 grains.

3.3 Application to Dual Phase Alloy Models

As was emphasized in [Hasebe (2004)b], one of the strongest features of the field theory, especially regarding the “field fluctuation” viewpoint, is the applicability to more complicated and realistic situations beyond single phase cases. The immediate example would be dual phase alloy model containing hard grains with various volume fractions and morphologies.

Introducing these “heterogeneity” significantly enhances the field fluctuations [Hasebe (2004)b]. Particularly, the

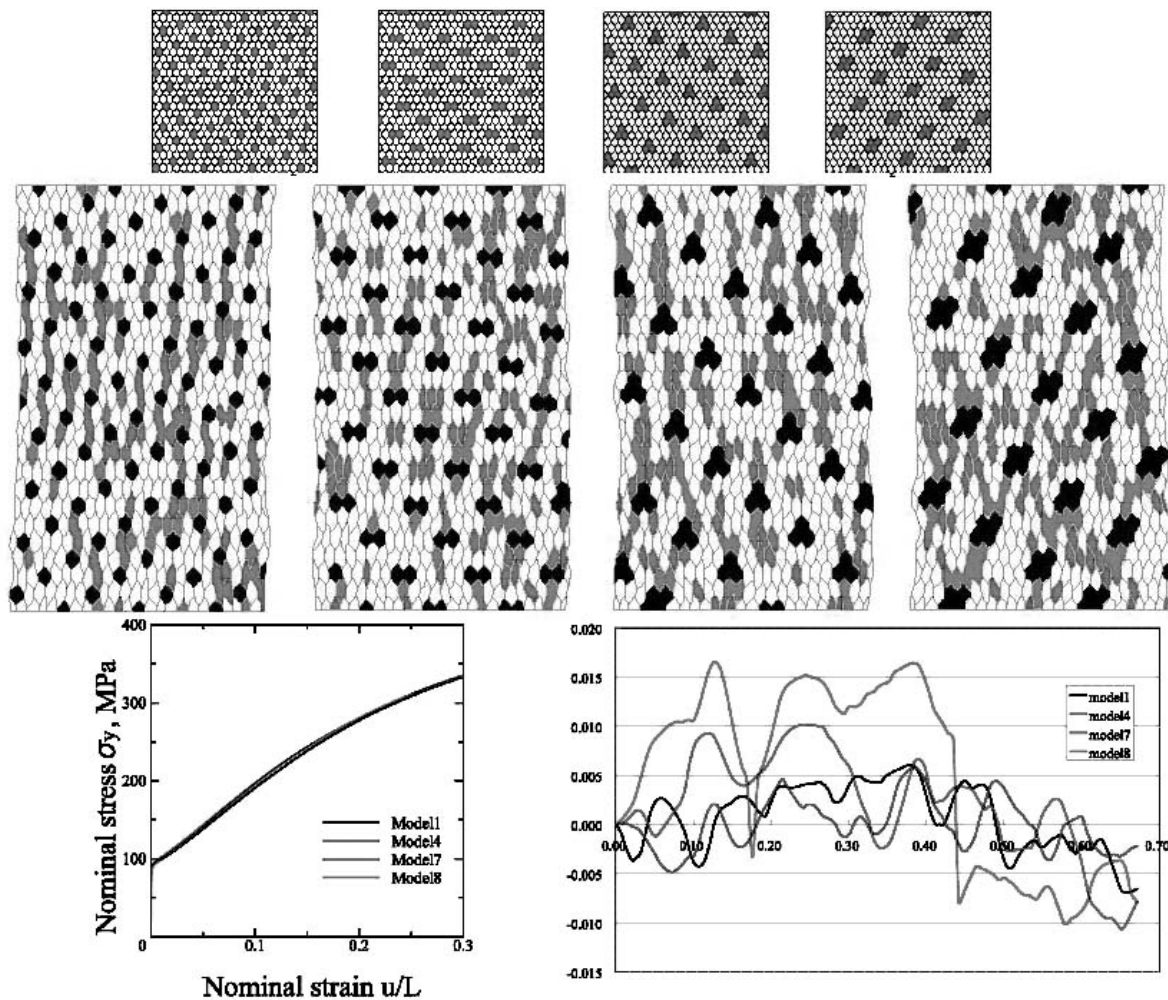


Figure 9 : Example of DP model simulations.

fluctuation of volumetric strain, which is negligibly small for single phase model, becomes larger according to the greatly enhanced fluctuation in the hydrostatic stress. Further details can be found in [Hasebe (2004b)].

Figure 9 represents dual distributions of hydrostatic stress and deviatoric (equivalent) strain for dual phase models with 15% hard phase (HP) volume fraction. Comparison of the figures clearly shows that even with a same HP volume fraction we have different duality distributions depending on the HP morphology. Clustering of the HP results in clustered duality distribution of hydrostatic stress and deviatoric strain, and it resultantly produces rougher surface morphology as shown in the insert in Fig.9. Interestingly the corresponding averaged stress-strain curves almost coincide regardless of the above differences, which tends to mislead us to a conclusion that the response of dual phase models is not basically influ-

enced by the difference in the HP distribution.

4 Crystal Plasticity Modeling

4.1 Constitutive Framework

In combining all the aspects discussed above, the well-documented framework of crystal plasticity framework can be tentatively used. Started from Orwan's equation combined with the Arrhenius type expression for mean dislocation velocity, a physically sound constitutive framework can be derived. For BCC metals, a modified Kocks-Mecking model has been proposed by the author, which can accommodate several activation mechanisms at the same time such as those attributed to Peierls potential, dislocation processes and foreign obstacles for the effective stress components. The idea here is to distinguish the main effective stress component controlling

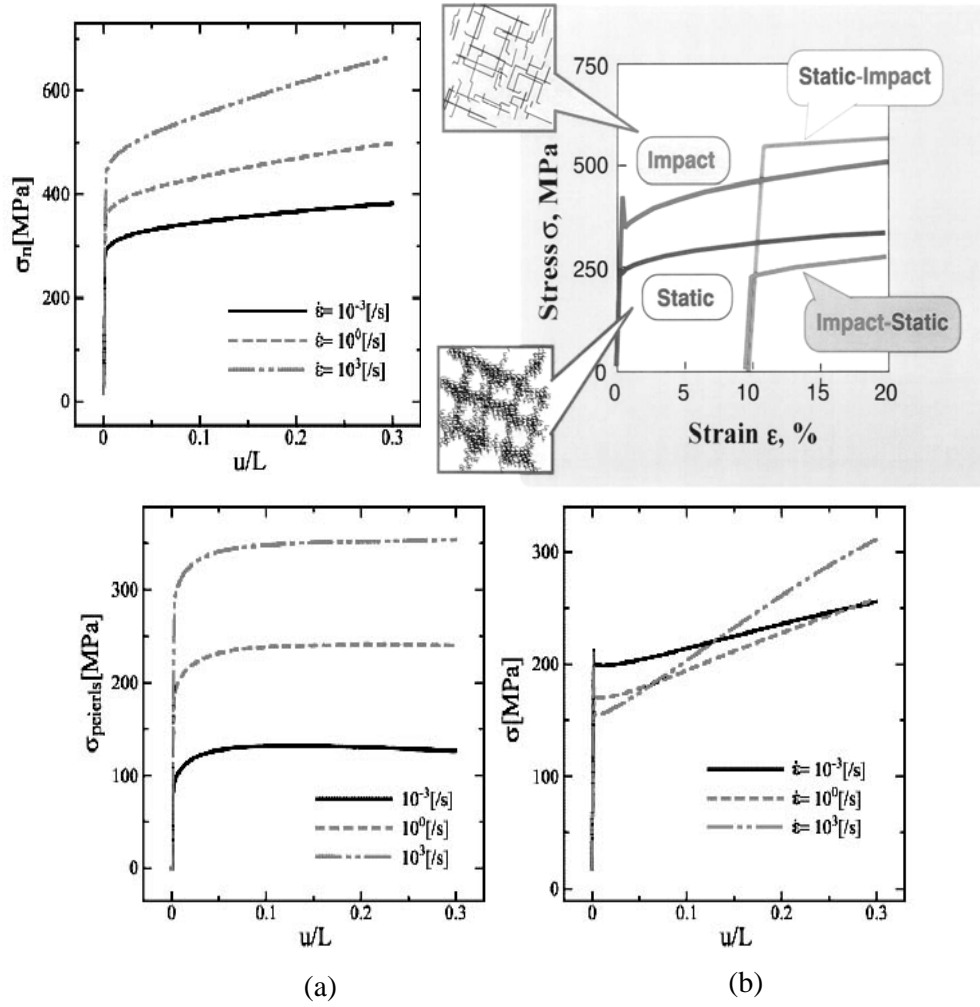


Figure 10 : Simulated stress-strain curves for BCC iron under three strain rates, together with effective stress components for (a)Peierls potential and (b)dislocation processes. Insert shows results reproducing “negative” strain rate history effect.

the constitutive behavior from the others which are basically kept constant during deformation. The explicit form is given by,

$$\tau = (\tau_1^* + \tau_2^* + \dots + \tau_n^*) + \tau_i$$

$$\Leftrightarrow \tau_1^* = \langle \tau - (\tau_2^* + \dots + \tau_n^*) \rangle - \tau_i \quad (8)$$

where τ_1^* represents the effective stress essentially evolves during deformation. τ_1^* is used for the activation energy function as,

$$\Delta G = \Delta G_0 \left[1 - \left(\frac{\tau_1^*}{\tau_1^*} \right)^p \right]^q \quad (9)$$

Substituting this into Orowan’s equation, we have,

$$\dot{\gamma} = \dot{\gamma}_0 \exp \left[-\frac{\Delta G_0}{kT} \left\{ 1 - \left(\frac{\langle \tau - (\tau_2^* + \dots + \tau_n^*) \rangle - \tau_i}{\tau_1^*} \right)^p \right\} \right]^q \quad (10)$$

Expression for the Peierls potential term, for example, is give by,

$$\tau_2^* = \left[1 - \left(\frac{kT}{G_0 \mu b^3} \ln \frac{\dot{\gamma}_{02}}{\dot{\gamma}} \right)^{1/q_2} \right]^{1/p_2} \quad (11)$$

If there is strong correlations among the processes, Eq.(8) is extended to be,

$$\tau_1^* = \left\langle \{ (\tau)^2 - (\tau_{strong}^*)^2 \}^{1/2} - (\tau_2^* + \dots + \tau_n^*) \right\rangle - \tau_i$$

(12)

Figure 10 displays an example of the results for Fe under various strain rates up to impact loading region.

The constitutive framework given here successfully reproduces the strain rate dependency of stress response mainly resulted from that of thermal activation process overcoming Peierls potential (see Fig.10(a)). Effective stress for dislocation processes (Fig.10(b)) exhibits a reversed trend in relatively small strain region, which will partially attribute to the “negative” strain rate history effect. Further details as well as updated results will be provided in a coming paper.

4.2 Hardening Evolution Models

Figure 11 summarizes the hardening evolution models forming the essential parts of the present constitutive model, which is roughly composed of evolution equations for drag stress $K^{(\alpha)}$ and back stress $\Omega^{(\alpha)}$ [Hasebe, Kumai and Imaida (1998b)] given respectively by,

$$\begin{aligned} \dot{K}^{(\alpha)} &= Q_{\alpha\beta} H(\gamma) \left| \dot{\gamma}^{(\alpha)} \right| \text{ and } \dot{\Omega}^{(\alpha)} \\ &= -A_{cell} \left\{ \langle d_{cell}^* - \bar{x}_N \rangle + \alpha \right\}^{-2} \end{aligned} \quad (13)$$

where $H(\gamma)$ is hardening modulus for a referential stress-strain curve. Hardening ratio $Q_{\alpha\beta}$ is given by,

$$Q_{\alpha\beta} = \delta_{\alpha\beta} + f_{\alpha\kappa} S_{\kappa\beta} + \delta^{\alpha\beta} \sum_k F_k(\alpha_k^{(\beta)}, \eta_k^{(\beta)}) \quad (14)$$

where $f_{\alpha\kappa}$ represents dislocation interaction matrix, and $S_{\kappa\beta}$ expresses history matrix further given as a function of plastic work done by the effective stress responsible for dislocation processes. $F_k(\alpha_k^{(\beta)}, \eta_k^{(\beta)})$ expresses the field theoretical “strain gradient terms” described below.

The hardening ratio $Q_{\alpha\beta}$ provides the evolution of dislocation cell structure during plastic deformation, which is given as a function of plastic work activated by dislocation-dislocation interaction. The use of plastic work instead of slip strain has been motivated by a fact that impact loading, under which larger flow stress results, yields finer and denser dislocation cells comparing with static loading for FCC and HCP metals. This implies that such dislocation substructure evolution is driven not only by the amount of slip but also by the imposed stress level. The difference in the evolved cell structures depending on strain rate leads to different

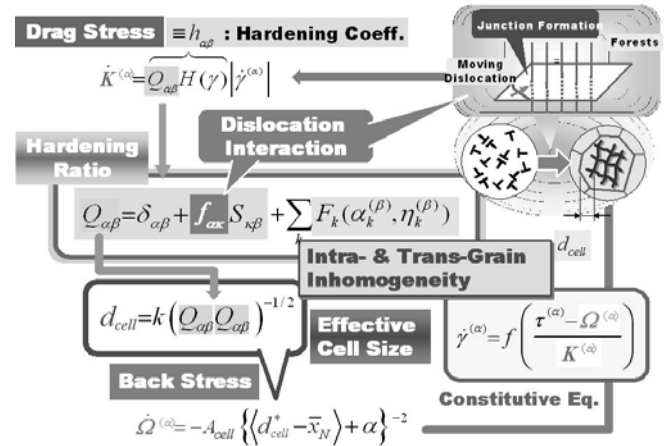


Figure 11 : Construction of constitutive model proposed based on field theory of plasticity characterized by “hardening ratio.”

strain history effect known as strain rate history effect. FCC and HCP metals generally show “positive” strain rate history effect, whereas BCC metals exhibit the opposite trend, i.e., “negative” strain rate history effect. The latter can be described by using the effective stress for dislocation processes in evaluating the plastic work.

The hardening ratio has a physical meaning of reciprocal of dislocation mean free paths characterized by effective cell size. The effective cell size defined here represents the piling-up distance against which subsequently moving dislocations are blocked producing long range back stress field in the cell interior regions. Therefore, the effective cell size is used in the back stress evolution model.

Figure 12 displays a set of examples of the results obtained in a series of simulations for cyclic non-proportional (NP) loading for SUS304 stainless steel [Hasebe and Imaida (1999b)]. Variation of additional hardening with various non-proportional strain paths is successfully reproduced together with corresponding cell evolutions. Figure12(a) shows comparison of cyclic stress among basic NP strain paths, i.e., cruciform, square and circle, with that under proportional path, demonstrating marked additional hardening depending on the path. The saturated cyclic stresses are quantitatively compared with experimental results in Fig.12(b) on the normalized basis with that for the proportional path. The comparison shows overall agreement. Figure 12(c) shows simulated stress responses for stair-step

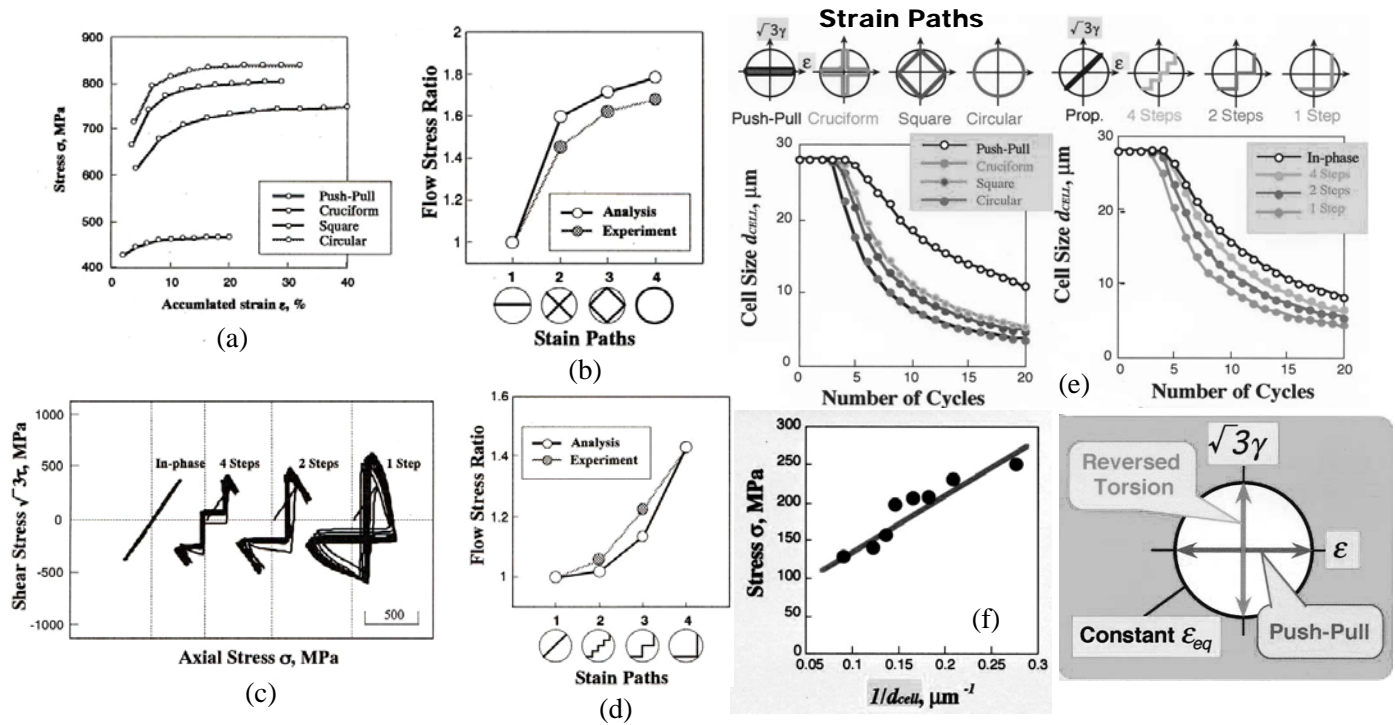


Figure 12 : Examples of simulation results for additional hardening under non-proportional cyclic loading for SUS304 stainless steel.

NP strain paths as examples of more complicated cases. Same comparison as in Fig.12(b) is made in Fig.12(d) showing also good agreement with experiments. Corresponding cell size evolutions with strain for all the strain paths are presented in Fig.12(e), while the reciprocal of the cell sizes are correlated with the cyclic stresses in Fig.12(f). The latter demonstrate that a similitude-like correlation holding between cell size and cyclic stress is roughly reproduced by the present model.

4.3 Field Theory Based Strain Gradient Terms

Since the hardening ratio $Q_{\alpha\beta}$ described above physically means the inverse of the effective cell size, inhomogeneities in strain distribution described by differential geometrical quantities will promote or restrict the evolution. The dislocation density tensor expresses that dislocations excessively exist where there are distributions in plastic strain. The incompatibility tensor, on the other hand, expresses fields where dislocation density spatially varies. Introducing the strain gradient terms is straightforward if the mean spacing of dislocations or defects is proportional to the cell size. Effective distances of moving dislocations due to the strain gradients will be in pro-

portion to the mean spacing of dislocations specified by the densities expressed by the two tensors $\alpha_k^{(\beta)}$ or $\eta_k^{(\beta)}$ based on an empirical observation. The proportionality constants are assumed to be proportional to the grain size given and take values with orders of 10 to 100.

A simple interpretation of dislocation and defect densities that the inverse of their square root means their mean spacing, together with the above assumption leads to the following explicit expressions for the related strain gradient terms, i.e.,

$$F(\alpha^{(\alpha)}) = k \cdot d_{cell}^{\alpha^{(\alpha)}-1} = \frac{k}{p_\alpha} \left(\frac{|\alpha^{(\alpha)}|}{b} \right)^{1/2}$$

$$F(\eta^{(\alpha)}) = k \cdot d_{cell}^{\eta^{(\alpha)}-1} = \text{sgn}(\eta^{(\alpha)}) \cdot \frac{k}{p_\eta} \left(\frac{l_{defect}}{b} |\eta^{(\alpha)}| \right)^{1/2} \quad (15)$$

where k means initial cell size normally coinciding with initial grain size.

The physical manifestations of these gradient terms can be easily seen from Fig.13 where distributions of the two

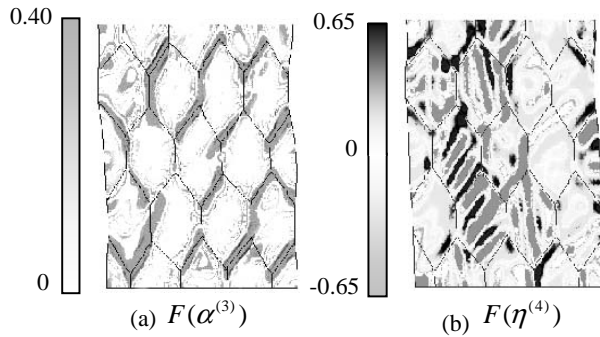


Figure 13 : Contour diagrams representing (a)alpha- and (b)eta-terms

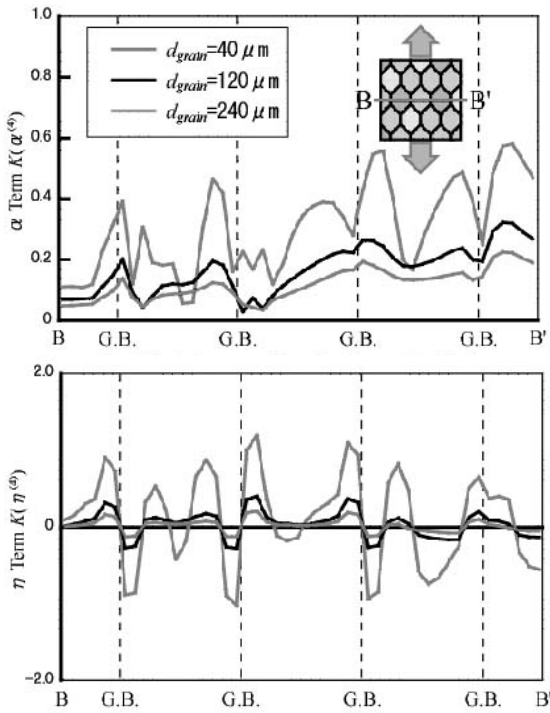


Figure 14 : Grain size dependence of strain gradient term variations.

terms are shown. As shown in Fig.13(a), $F(\alpha^{(\alpha)})$ yields “geometrically-necessary” type accommodation of deformation among grains, whereas $F(\eta^{(\alpha)})$ causes modulation over plus and minus signs within grains for particular crystallographic orientations (Fig.13(b)). These results demonstrate the modulation of the incompatibility term $F(\eta^{(\alpha)})$ causes further modulations of stress, strain fields and cell size. Because the modulation occurs when a multiple slip takes place in a single slip plane, it can be regarded as a candidate for a “microband” or “matrix

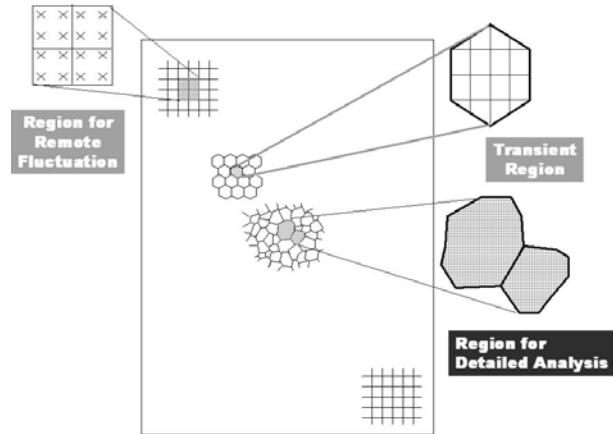


Figure 15 : Convenient model for multi-scale polycrystalline plasticity simulation.

band” model, although there are several definitions of the microband itself in the literature, which needs further discussion.

Scale effects relating to the substructure evolutions can be expressed by the model. Figure 14 shows comparison of $F(\alpha^{(\alpha)})$ and $F(\eta^{(\alpha)})$ among three initial grain sizes, i.e., 40, 120 and 240 micrometers. Both the terms mainly promote the cell refinement when the grain size decreases, which is experimentally conformed.

Based on the findings provided above, a convenient polycrystal simulation model can be proposed as illustrated in Fig.15. The model is composed roughly of three regions for precise analysis, global fluctuation and their transition, each of which has different number of mesh divisions depending on the purposes. If we need precise information on the surface inhomogeneity, for example, the first region should be simply placed there. One of the advantages of this model would be that it requires much lower computational cost in simulating multiple scale phenomena without a need of any coupling calculation.

5 Concluding Remarks

A bird’s-eye-view of the field theoretical studies conducted in recent years is briefly presented. Overview of field theory of plasticity promoted mainly by the author’s group are presented first with some emphasis on key concepts. Secondly the application examples to polycrystalline plasticity are given showing several of the updated results particularly about “collective” effects of large

number of composing grains, which seems to be absent in any other approaches so far. A constitutive framework combined with field theoretical strain gradient terms is discussed next, demonstrating prediction ability of additional hardening under complex loading as a framework, together with potentials in describing intra-granular inhomogeneities like microbands and matrix bands.

References

- Ghoniem, N. M. and Cho, K.J.** (2002): The Emerging Role of Multiscale Modeling in Nano- and Micro-mechanics of Materials, *ibid.*, Vol. 3, No. 2, pp. 147-174
- Ghosh, S.** (2002): Computational Material Modeling: A Current Perspective, *CMES: Computer Modeling in Engineering and Sciences*, Vol. 5, No. 1, pp. 1-4.
- Hasebe, T.; Imaida, Y.** (1998): Construction of Quantum Field Theory of Dislocations Based on the Non-Riemannian Plasticity, *Acta. Metall. Sinica*, , Voll.11, No.6, pp.405-411.
- Hasebe, T., Kumai, S. and Imaida, Y.** (1998): Impact Compression Behavior of FCC Metals with Pre-Torsion Behavior, *J. Maters. Process. Technol.*, Vol. 85, pp.184-187.
- Hasebe, T.; Imaida, Y.** (1999a): Gauge Field Theory of Dislocations and the Non-Riemannian Plasticity, *Mechanical Behavior of Materials*, Vol.III, pp.1077-1082.
- Hasebe, T.; Imaida, Y.** (1999b): Dislocation Pileup Model for Back Stress Evolution in Crystalline Plasticity, *Trans. Struct. Maters. Reactor Technol.* Vol. 15, pp.801-808.
- Hasebe, T.** (2004a): Continuum Description of Inhomogeneously Deforming Polycrystalline Aggregate based on Field Theory, Mesoscopic Dynamics of Fracture Processes and Materials Strength (*Proc. IUTAM Symp.*), Eds. H. Kitagawa, Y. Shibutani, Kluwer, pp.381-390.
- Hasebe, T.** (2004b): Field Theoretical Multiscale Polycrystal Plasticity, Vol. 29, No.8, *MRS-J*, pp.3619-3624.
- Thomson, R., Levine, L. E., Shim, Y., Savage, M. F. and Kramer, D. E.** (2002): A Multi-Scale Theoretical Scheme for Metal Deformation, *CMES: Computer Modeling in Engineering and Sciences*, Vol. 3, No. 2, pp. 245-254.
- Zbib, H. M. and Diaz de la Rubia, T.**(2002): A multiscale model of plasticity *Int .J. Plasticity*, Vol.18, pp.1133-1163.

